Model for Reaction-Assisted Polymer Dissolution in LIGA

Richard S. Larson

Fluid and Thermal Science Department, Sandia National Laboratories, Livermore, California 94551-0969

Received 3 March 2004; accepted 8 October 2004
DOI 10.1002/app.21722
Published online in Wiley InterScience (www.interscience.wiley.com).

ABSTRACT: A new chemically oriented mathematical model for the development step of the LIGA process is presented (LIGA is an acronym for the German words *Lithographie*, *Galvanoformung*, and *Abformung*). The key assumption is that the developer can react with the polymeric resist material to increase the solubility of the latter, thereby partially overcoming the need to reduce the polymer size. The ease with which this reaction takes place is assumed to be determined by the number of side-chain scissions that occur during the X-ray exposure phase of the process. The dynamics of the dissolution process are simulated by the solution of the reaction diffusion equations for this three-component, two-phase system, the three species being the unreacted and reacted polymers and the solvent. The mass fluxes are described by multicomponent diffusion (Stefan–Maxwell) equations, and the chemical potentials are assumed to be given by the Flory–Huggins theory. Sample calculations are used to determine the dependence of the dissolution rate on key system parameters such as the reaction rate constant, polymer size, solid-phase diffusivity, and Flory–Huggins interaction parameters. A simple photochemistry model is used to relate the reaction rate constant and the polymer size to the absorbed X-ray dose. The resulting formula for the dissolution rate as a function of the dose and temperature is fit to an extensive experimental database to evaluate a set of unknown global parameters. The results suggest that reaction-assisted dissolution is very important at low doses and low temperatures, the solubility of the unreacted polymer being too small for it to be dissolved at an appreciable rate. However, at high doses or at higher temperatures, the solubility is such that the reaction is no longer needed, and dissolution can take place via the conventional route. These results provide an explanation for the observed dependences of both the rate of dissolution and its activation energy on the absorbed dose. J Appl Polym Sci 97: 25–37, 2005

Key words: lithography; miscibility; modeling; photochemistry

INTRODUCTION

LIGA (an acronym for the German words *Lithographie*, *Galvanoformung*, and *Abformung*) is an emerging process for the fabrication of high-aspect-ratio microstructures. The lithography step actually involves two separate tasks. A thick film of a poly(methyl methacrylate) (PMMA) resist material is first exposed to synchrotron X-rays through a patterned absorber mask, and the exposed areas are then developed (dissolved) by immersion in the so-called GG developer, which is a complex mixture of four liquid chemicals. The resulting trenches are then filled with a suitable metal or alloy by electrodeposition, the remaining PMMA is dissolved in a strong solvent, and the finished metal part is used as a template for mass production. LIGA has great promise for the efficient fabrication of microparts, but a good deal remains to be done in the areas of process improvement and optimization. Much of the progress to this point has been achieved through experimentation and empiricism, and it is clearly desirable to have a more fundamental understanding of the physics and chemistry involved. This applies particularly to the polymer dissolution step, which is the primary focus of this article.

It has long been known that the process of polymer dissolution involves more than simple mass transfer at the solid–liquid interface. The complication arises from the fact that a polymer molecule cannot be released from the solid phase until its entanglements with other molecules have been relaxed or broken. Furthermore, the polymer generally has a finite capacity to imbibe a solvent. Therefore, the first step in the dissolution process is the penetration of solvent molecules into the polymer matrix; this gives rise to a swollen gel layer in which the polymer fragments are more mobile. These fragments can then diffuse to the interface and pass into the liquid phase. There may or may not be a sharp demarcation between the gel and dry polymer (glass) layers; if there is, then of course one must deal with the existence of three separate phases.

Although this qualitative picture of polymer dissolution is generally accepted, attempts to model the

Sandia is a multiprogram laboratory operated by Sandia Corp., a Lockheed Martin company, for the U.S. Department of Energy's National Nuclear Security Administration under contract DE-AC04-94AL85000.

Correspondence to: R. S. Larson (rslarso@ca.sandia.gov).

process in any detail have been quite scarce, especially in the context of LIGA. The most comprehensive model proposed thus far is probably that of Papanu et al.[1,2] In their approach, transport in the gel layer is modeled as simple Fickian diffusion. An effective surface concentration at the gel–solvent interface is computed by the addition of an elastic term to the standard Flory–Huggins expression for the chemical potential, and the movement of this interface is governed by an equation involving the polymer disentanglement rate as estimated from reptation theory. For so-called case II penetration, in which there is a well-defined glass layer, the movement of the gel–glass interface is assumed to be related to the stress level in the polymer. A somewhat similar model was presented by Herman and Edwards,[3] who used the reptation model to estimate the stresses brought by solvent penetration into the polymer and then argued that the dissolution rate should be limited by stress relaxation. More recently, Hasko et al.[4] formulated a streamlined version of the Papanu model and used it with some success to describe the dissolution of PMMA in mixtures of methyl isobutyl ketone and isopropyl alcohol.

The foregoing models treat polymer dissolution as essentially a physical (rather than chemical) process, and they were not developed with LIGA in mind. Thus, they imply that a polymer will dissolve more quickly after irradiation simply because its molecular weight has been reduced. However, Schmalz et al.[5] presented strong evidence that the development step of LIGA is more complicated than this. First, they noted that an irradiated sample of PMMA will dissolve more quickly in the GG developer than a non-irradiated sample of the same molecular weight. They also noted that the dissolution rate is affected by the tacticity of the polymer, everything else being equal. In their view, the developer acts as more than just a solvent; it also initiates a chemical reaction with the polymer that converts the latter into a more soluble form. This reaction is thought to occur preferentially in irradiated parts of the polymer molecule, in which the nucleophilic developer has easier access because of scission of, or damage to, the ester side chains. If this scenario is correct, then a purely physical description of the dissolution process will not be adequate.

The purpose of this work is to formulate and solve a chemically oriented model for polymer dissolution that incorporates the ideas just described. First, a thermodynamically consistent set of governing equations for the multicomponent, multiphase dissolution process is derived. The equations are then solved numerically for a number of sample cases to determine the dependence of the dissolution rate on the key physical parameters. A simple photochemistry model is also proposed to relate the postexposure polymer properties to the absorbed radiation dose. This yields a rather complex expression for the dissolution rate as a function of the dose and the temperature, and the constants in this formula are evaluated by the fitting of the formula to an extensive experimental database. The results are analyzed to determine the relative importance of reaction-assisted dissolution under different exposure and development conditions.

MODEL FORMULATION

The model of reaction-assisted polymer dissolution to be presented here is based on two principal assumptions: (1) the removal or alteration of polymer side chains by X-ray irradiation during the exposure step leaves the polymer molecule susceptible to chemical attack by the developer solution, and (2) this chemical reaction converts the polymer into a new form that has greater solubility. Of course, another effect of the X-rays is to reduce the average molecular weight of the polymer via main-chain scissions, and this in itself can enhance the solubility; however, as already noted, there is compelling evidence that specific chemical effects are also involved. In any case, this model will reduce to one of purely physical dissolution if the rate constant for the chemical reaction is set to zero.

With these assumptions in mind, we can surmise that the first step in the dissolution process is, as usual, the diffusion or permeation of solvent molecules into the polymer matrix; this gives rise to the gel layer, which is a familiar feature of such systems. The volumetric (as opposed to interfacial) contact between the polymer and the developer then allows the aforementioned chemical reaction to take place at a rate that is determined by the local concentrations of both species. Both the original and converted forms of the polymer can diffuse across the gel layer and pass into the liquid phase, although the latter is favored because of its enhanced solubility. Finally, the dissolved polymer of either type diffuses across the liquid-phase boundary layer and is swept away into the bulk solvent. The loss of polymer molecules from the solid phase causes the solid (gel)–liquid interface to recede, and the speed with which it does so is defined as the development rate.

Although the GG developer that is normally used in LIGA is a mixture of four distinct chemicals, it will be treated as a single species with suitable average properties in this model. On the other hand, the original and converted forms of the polymer will be treated as distinct because the differences in their behavior are a crucial feature of the model. Thus, the analysis must describe multicomponent diffusion with a simultaneous chemical reaction in a three-component, two-phase system. (There is assumed to be no sharp demarcation between the gel layer and the dry, unreacted polymer, so they are treated as parts of the same solid phase.) Furthermore, the equations must account

for the highly nonideal nature of polymer–solvent mixtures, and the descriptions of diffusion and interfacial equilibrium must be thermodynamically consistent.

The basic governing equations for this system are the transient material balances for the three species present. As is customary in problems involving polymers, the model will be formulated in terms of volumetric variables, under the assumption that all processes are volume-conserving. In one dimension, the mass balances have the following form:

$$\frac{\partial \phi_i}{\partial t} + \frac{\partial N_i}{\partial z} = \dot{V}_i \tag{1}$$

where t is the time, ϕ_i is the volume fraction of species i, N_i is its volume flux with respect to fixed coordinates, $\dot{V}_i$ is its volumetric production rate, and z is the spatial coordinate normal to the interface. The absence of a convective term is due to the overall continuity equation and to the fact that the dry polymer is assumed to be attached to a stationary substrate. Because the equations for the three species are not all independent, only two of them need be solved. Letting subscripts 1, 2, and 3 denote the solvent, unconverted polymer, and converted polymer, respectively, we can arbitrarily choose to solve eq. (1) for $i = 1$ and $i = 2$.

Next, it is necessary to relate N_i to the composition gradients within the system. Because there are three components and because the mixture is expected to be highly nonideal, Fick's law is wholly inadequate; in its place, we use the volumetric version of the general multicomponent diffusion equation,[6] which is the analogue of the Stefan–Maxwell equation for gases:

$$\phi_i \frac{\partial \mu_i}{\partial z} = \frac{RT}{c} \sum_j \frac{1}{V_j \mathcal{D}_{ij}} (\phi_i N_j - \phi_j N_i) \tag{2}$$

where μ_i and V_i are the chemical potential and molar volume, respectively, of species i; D_{ij} is the true binary diffusion coefficient for species i and j; R is the universal gas constant; T is the absolute temperature; and c is the overall molar concentration of the mixture:

$$c = \sum_j \frac{\phi_j}{V_j} \tag{3}$$

Equation (2) can be inverted to give explicit expressions for the fluxes:

$$N_1 = \frac{1}{RT}\left(D_{12}\frac{\partial \mu_2}{\partial z} + D_{13}\frac{\partial \mu_3}{\partial z}\right) \tag{4}$$

where

$$D_{12} = \frac{cV_1}{\bar{\mathcal{D}}} \mathcal{D}_{12}\phi_2\left(\frac{1-\phi_1}{V_2}\mathcal{D}_{13} + \frac{\phi_1}{V_1}\mathcal{D}_{23}\right) \tag{5}$$

$$D_{13} = \frac{cV_1}{\bar{\mathcal{D}}} \mathcal{D}_{13}\phi_3\left(\frac{1-\phi_1}{V_3}\mathcal{D}_{12} + \frac{\phi_1}{V_1}\mathcal{D}_{23}\right) \tag{6}$$

$$\bar{\mathcal{D}} = \frac{\phi_1}{V_1}\mathcal{D}_{23} + \frac{\phi_2}{V_2}\mathcal{D}_{13} + \frac{\phi_3}{V_3}\mathcal{D}_{12} \tag{7}$$

It should be emphasized that coefficients D_{ij}, unlike $\mathcal{D}_{ij}$, are not symmetric in i and j.

To complete the formulation, the chemical potentials must now be expressed in terms of the volume fractions. This can be done with the multicomponent Flory–Huggins equations,[7] which involve as physical parameters the molar volume ratios, $m_{ij} \equiv V_i/V_j$, and a set of interaction parameters, χ_{ij}. Thus, for example,

$$\mu_1 = \mu_1^0(T) + RT[\ln \phi_1 + (1-\phi_1)(1 + \chi_{12}\phi_2 + \chi_{13}\phi_3) - m_{12}\phi_2 - m_{13}\phi_3 - m_{12}\chi_{23}\phi_2\phi_3] \tag{8}$$

where $\mu_1^0(T)$ is the chemical potential in the pure state. The expressions for μ_2 and μ_3 can be obtained simply by the permutation of the indices. Clearly, because m_{ji} is equal to $1/m_{ij}$ and m_{jk} is equal to $m_{ji}m_{ik}$, there are only two independent values of m. In addition, the Flory–Huggins theory shows that χ_{ji} is equal to $m_{ji}\chi_{ij}$, so the number of independent χ values is three. Furthermore, if these binary interaction parameters can be expressed in terms of individual solubility parameters in the manner indicated by Prausnitz,[8] then it can be readily shown that

$$\chi_{23} = m_{21}(\chi_{12}^{1/2} - \chi_{13}^{1/2})^2 \tag{9}$$

Thus, only χ_{12} and χ_{13} need be specified.

The substitution of the Flory–Huggins chemical potentials into eq. (4) for an isothermal system gives

$$N_1 = K_{11}\frac{\partial \phi_1}{\partial z} + K_{12}\frac{\partial \phi_2}{\partial z} \tag{10}$$

where

$$K_{11} = D_{13}\left[-\frac{1}{\phi_3} + 1 + (1-\phi_3+\phi_1)\chi_{31} - m_{31} + \chi_{32}\phi_2 - m_{32}\bar{\mathcal{D}}_{21}\phi_2\right] + D_{12}[(1-\phi_2)(\chi_{21}-\chi_{23}) + m_{23}\chi_{31}(\phi_1-\phi_3) - m_{23} - m_{21}] \tag{11}$$

$$K_{12} = D_{13}\left[-\frac{1}{\phi_3} + 1 + (1 - \phi_3 + \phi_2)\chi_{32} - m_{32} + \chi_{31}\phi_1 - m_{32}\chi_{21}\phi_1 \right] + D_{12}\left[\frac{1}{\phi_2} - 1 - (1 + \phi_3 - \phi_2)\chi_{23} + m_{23} - \chi_{21}\phi_1 + m_{23}\chi_{31}\phi_1 \right] \quad (12)$$

The corresponding expression for N_2 can be obtained by the interchanging of indices 1 and 2 in eqs. (10), (11), (12), (5), and (6). N_1 and N_2 are then given in terms of gradients of ϕ_1 and ϕ_2 alone, as required. Obviously, the flux equations are far more complicated than those that would have been obtained by the simple application of Fick's law.

To complete the system of governing equations, we need an expression for the homogeneous reaction rate $\dot{V}_i$ in eq. (1). Although the precise nature of the reaction is not known, the rate of any attack of the solvent on the exposed polymer should depend on the local concentrations of both species. In the absence of any information to the contrary, it is simplest to assume that each dependence is first-order:

$$\dot{V}_1 = -k\phi_1\phi_2 \quad (13)$$

Here k is a rate constant that presumably depends on both the temperature and the extent of damage done to the polymer by X-ray irradiation. Because $\dot{V}_i$ is a volumetric reaction rate, the corresponding expression for $\dot{V}_2$ is

$$\dot{V}_2 = -m_{21}k\phi_1\phi_2 \quad (14)$$

The system consisting of eqs. (1) and (10), written for both species 1 and species 2, can now in principle be solved. The progressive dissolution of the polymer layer is, of course, a time-dependent process; however, we are interested primarily in the situation in which the solid–liquid interface recedes at a steady rate. In such a case, the governing equations should be time-independent when written in a coordinate system attached to the interface, as long as there is a significant expanse of dry polymer between the gel layer and the substrate. This suggests that we introduce a similarity variable $\eta = z - ut$, which measures the distance from the interface, the assumption being that the volume fractions and fluxes will depend on η alone and not on z and t individually. The (constant) interfacial velocity u is not known *a priori* and must be determined as part of the solution to the problem. (Of course, because the interface moves to the left as the polymer dissolves, the computed value of u will be negative, so the dissolution rate is $v = -u$.) It is also useful to introduce fluxes $J_i = N_i - u\phi_i$ with respect to the moving interface. In terms of the new variables, the equations to be solved become

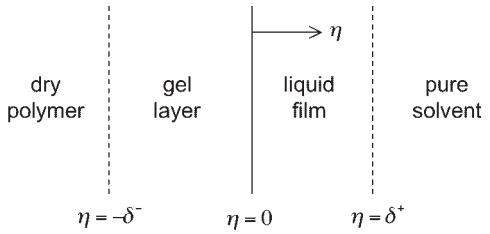

Figure 1 Geometrical configuration used for the analysis of polymer dissolution.

$$\frac{dJ_1}{d\eta} = -k\phi_1\phi_2 \quad (15)$$

$$\frac{dJ_2}{d\eta} = -m_{21}k\phi_1\phi_2 \quad (16)$$

$$J_1 = K_{11}\frac{d\phi_1}{d\eta} + K_{12}\frac{d\phi_2}{d\eta} - u\phi_1 \quad (17)$$

$$J_2 = K_{21}\frac{d\phi_1}{d\eta} + K_{22}\frac{d\phi_2}{d\eta} - u\phi_2 \quad (18)$$

We must still specify the boundary conditions for the problem. Because there are four first-order differential equations in each of two phases, it might appear that eight such conditions are required. However, because the interfacial velocity u is not known, one additional boundary condition is needed to fix its value, and u can be termed an eigenvalue of the problem. We obtain four of the necessary boundary conditions by specifying the mixture compositions at the outer edges of the problem domain. Referring to Figure 1, we must have the pure solvent at the right-hand edge of the liquid-phase boundary layer, so

$$\phi_1(\delta^+) = 1 \quad (19)$$

$$\phi_2(\delta^+) = 0 \quad (20)$$

Likewise, because there is dry, unconverted polymer in the region to the left of the gel layer, we have

$$\phi_1(-\delta^-) = 0 \quad (21)$$

$$\phi_2(-\delta^-) = 1 \quad (22)$$

An important distinction between the layer thicknesses δ^+ and δ^- should be noted. Whereas the former is regarded as a real physical quantity whose value is determined by the hydrodynamics (e.g., stirring) in the bulk liquid, the latter is an artificial quantity that is

introduced for computational convenience. In principle, boundary conditions (21) and (22) should be applied at $\eta = -\infty$, and in practice δ^- must be so large that any further increase in its value causes no change in the solution. This approach ensures that all fluxes with respect to fixed coordinates are zero in the dry polymer layer, as they must be.

The remaining five boundary conditions are imposed at the solid–liquid interface. The fluxes relative to this interface must be continuous, so

$$J_1(0^-) = J_1(0^+) \tag{23}$$

$$J_2(0^-) = J_2(0^+) \tag{24}$$

On the other hand, the volume fractions will not be continuous at $\eta = 0$. As is customary, we assume that the two phases are in thermodynamic equilibrium at this point, and so the chemical potential of each species is continuous:

$$\mu_1(0^-) = \mu_1(0^+) \tag{25}$$

$$\mu_2(0^-) = \mu_2(0^+) \tag{26}$$

$$\mu_3(0^-) = \mu_3(0^+) \tag{27}$$

The chemical potentials are evaluated from eq. (8) and its analogues, with ϕ_3 everywhere replaced by $1 - \phi_1 - \phi_2$. Equations (25)–(27) are all independent, so each of them must be imposed to satisfy the condition of equilibrium. On the other hand, the analogue of eqs. (23) and (24) for species 3 would be redundant because the fluxes J_i always sum to a constant, namely, $-u$.

SOLUTION METHOD

The nonlinear boundary value problem, consisting of eqs. (15)–(27), presents a significant computational challenge. The most straightforward approach is to write the differential equations in finite-difference form and to use a packaged routine to solve the resulting large system of algebraic equations. Unfortunately, this method seems to be incapable of resolving (with a reasonable number of grid points) the extremely sharp concentration gradients that are typically observed, even when adaptive meshing is employed. The alternative is to use a shooting method, in which the differential equations for each phase are integrated numerically from one side to the other, and any unknown initial values or parameters that are needed for the integrations are guessed and then adjusted to satisfy the boundary conditions at the endpoints. This method also involves several difficulties, however. First, the numerical integrations tend to be unstable, in the sense that modest errors in the guessed quantities can cause a computed solution to blow up before the endpoint is reached. Obviously, this can require the initial guesses to be quite accurate, so the iteration process is not as robust as one would like. Second, if the iteration is fully automated via a nonlinear system solver, then one or more of the unknown interfacial volume fractions can become negative, and this will also cause the computation to fail [cf. eq. (8)]. This has led to the adoption of a two-tier shooting method, which will now be described.

For specified values of the physical parameters for the problem (in particular, the Stefan–Maxwell diffusivities, the reaction rate constant, and the Flory–Huggins parameters), the first step in the computation is to guess a value for $\phi_2(0^+)$. This is the quantity that is to be adjusted in the outer loop of the shooting method. For the chosen value, equilibrium relations (25)–(27) are then solved via the SLATEC routine DNSQE to find $\phi_2(0^-)$, $\phi_1(0^+)$, and $\phi_1(0^-)$, so that all of the interfacial volume fractions are known (tentatively). The remaining three quantities that are needed to carry out the numerical integrations, namely, $J_1(0)$, $J_2(0)$, and u, are then estimated; these are the adjustable parameters in the inner loop of the shooting method. The stiff equation solver DASSL[9] is used to integrate eqs. (15)–(18) outward from $\eta = 0^+$ to $\eta = \delta^+$ and also from $\eta = 0^-$ to $\eta = -\delta^-$. The SLATEC routine DNSQ is then used to adjust $J_1(0)$, $J_2(0)$, and u to satisfy exterior boundary conditions (19)–(21). The remaining condition, eq. (22), is satisfied in the outer loop by iteration on $\phi_2(0^+)$. This is accomplished via the SLATEC root finder DFZERO, which allows the user to place bounds on the solution; this eliminates the danger of taking the logarithm of a negative argument in the equilibrium relations. Finally, the entire process is repeated for progressively larger values of δ^- until the solution (in particular, the value of u) shows no further change.

SAMPLE RESULTS

The procedure just described allows one to compute the dissolution rate $v = -u$ for any set of values of the physical parameters characterizing the system. Of course, most (if not all) of these parameters will not be known *a priori*, so it will be necessary at some point to fit the model predictions to experimental data. Because v is generally reported as a function of the development temperature and the absorbed X-ray dose, two steps must be taken before the fitting procedure can be carried out. First, model results must be computed for a number of test cases to infer the quantitative relationship between v and the key physical parameters. Next, separate submodels must be used to relate these parameters to the temperature and the dose. The first of these tasks will now be discussed.

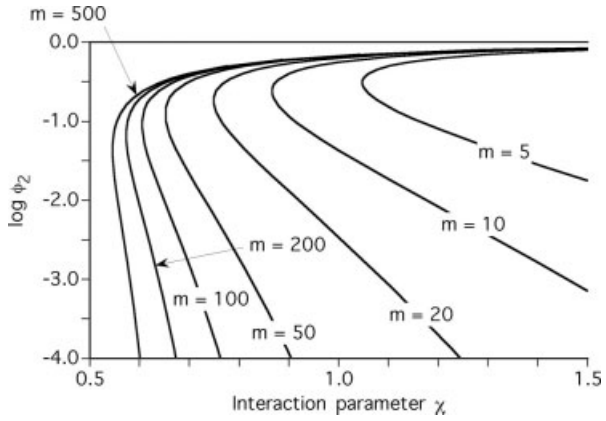

Figure 2 Equilibrium phase compositions for a solvent–polymer system from the Flory–Huggins theory.

It follows from the model formulation that dissolution rate v will depend on the following parameters: m_{21}, m_{31}, $\mathcal{D}_{12}$, $\mathcal{D}_{13}$, $\mathcal{D}_{23}$, χ_{12}, χ_{13}, k, and δ^+. A few simple approximations can be made to reduce the size of this list. First, because the postulated chemical reaction does not alter the length of the polymer chain, it is reasonable to take $m_{21} = m_{31} \equiv m$ and $\mathcal{D}_{12} = \mathcal{D}_{13} \equiv \mathcal{D}$. Actually, $\mathcal{D}$ can in general be a function of the mixture composition, and one would certainly expect to observe different values in the gel and liquid layers. Therefore, we take $\mathcal{D}$ to be piecewise constant, with values $\mathcal{D}^+$ and $\mathcal{D}^-$ for $\eta > 0$ and $\eta < 0$, respectively. The polymer–polymer diffusivity $\mathcal{D}_{23}$ should be unimportant by comparison; in the absence of further information, we take $\mathcal{D}_{23} = \mathcal{D}/m^{1/2}$ in each phase. Finally, for sample calculations, δ^+ and $\mathcal{D}^+$ can be set equal to unity with no loss of generality, as this merely serves to set the length scale and timescale for the problem. In other words, each of the remaining parameters becomes a dimensionless quantity (if it is not already) scaled by the characteristic length δ^+, the characteristic time $\delta^{+2}/\mathcal{D}^+$, or both. In this way, the list of parameters to be investigated is reduced to m, $\mathcal{D}^-$, χ_{12}, χ_{13}, and k.

Before the results of the dissolution simulations are shown, it is necessary to digress for a discussion of polymer solubility, as this is one of the crucial features of the model. Within the context of the Flory–Huggins theory, the solubility of a single polymer in a given solvent depends entirely on the values of $m_{21} \equiv m$ and $\chi_{12} \equiv \chi$, as determined by the solutions to eqs. (25) and (26). The form of this dependence is shown in Figure 2, which is a more detailed version of Figure XX-13 in ref. 10 Each curve gives the values (if any) of ϕ_2 in equilibrated liquid and solid phases as functions of χ for a fixed value of m. Because m is a rough measure of the polymer chain length, the plot shows that the polymer solubility increases very rapidly as the molecular weight decreases, whereas the nominally solid phase contains a significant amount of solvent. However, the solubility also increases very rapidly as χ decreases and the two chemical species become more compatible. In fact, if χ is sufficiently small, then the polymer and the solvent are miscible in all proportions, and for $\chi < 0.5$, this is true, regardless of the polymer molecular weight. Our model assumes that both of these avenues for improving solubility are operative in LIGA: chain scissions brought about by the X-rays obviously reduce the molecular weight, whereas the chemical reaction between the polymer and the developer lowers the value of χ.

Actually, because both the unconverted and converted forms of the polymer are present simultaneously during the development process, the equilibrium plot in Figure 2 is not sufficient to represent the situation; instead, a standard ternary phase diagram is needed. A typical example, as computed from eqs. (25)–(27), is shown in Figure 3. Here the Flory–Huggins parameters are fixed, and the diagram gives, for any overall mixture composition, the number of phases present at equilibrium as well as their individual compositions. For any point outside the dome-shaped region, there is only one phase, and thus there is complete miscibility of the three components. Within the dome, the system splits into two phases, the compositions of which are given by the ends of a tie line passing through the original point; the set of tie lines can be constructed from the conjugate line, as indicated. Polymer 3 by itself is miscible in all proportions with the solvent, whereas polymer 2 is not, in agreement with Figure 2. The fact that even small amounts of polymer 2 tend to give rise to incomplete miscibility suggests that a dissolution process involving these species will show a well-defined solid–liquid interface, which is an assumed feature of the model.

Returning now to the dynamics of dissolution, Figure 4 shows computed concentration profiles for a representative case. The Flory–Huggins parameters are the same as those in Figure 3; the solid-phase

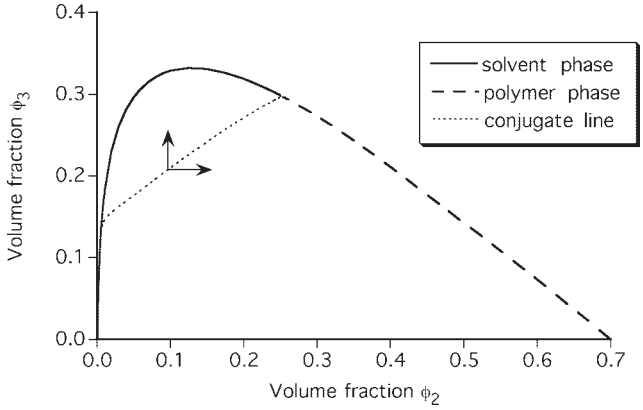

Figure 3 Ternary phase diagram for a single-solvent/dual-polymer system ($m = 20$, $\chi_{12} = 1.1$, $\chi_{13} = 0.7$).

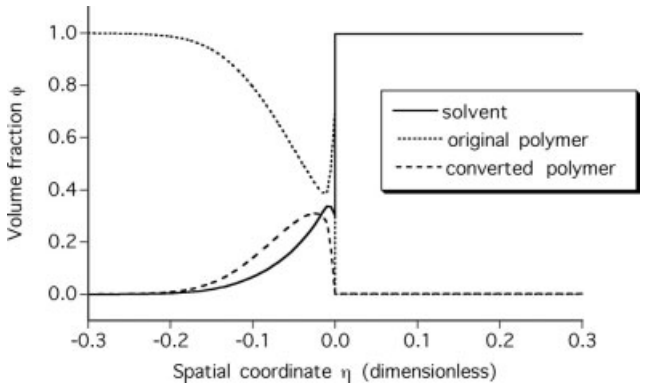

Figure 4 Steady-state concentration profiles for reaction-assisted dissolution ($m = 20$, $\chi_{12} = 1.1$, $\chi_{13} = 0.7$, $\mathcal{D}^- = 10^{-4}$, $k = 0.01$).

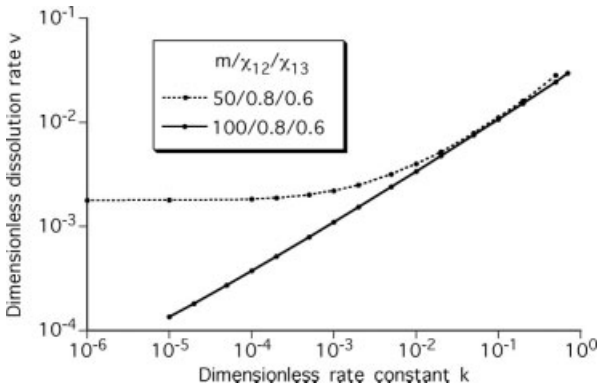

Figure 6 Computed dissolution rate v as a function of reaction rate constant k for $\mathcal{D}^- = 10^{-5}$, $\chi_{12} = 0.8$, $\chi_{13} = 0.6$, and two different values of m.

diffusivity is four orders of magnitude smaller than that in the liquid, and the reaction rate constant has a modest but surprisingly influential value. Obviously, both forms of the polymer have very low concentrations in the liquid phase, so the tie line representing the interfacial compositions is very close to the horizontal axis in Figure 3. Instead of rising smoothly from its equilibrium value at $\eta = 0^{-1}$ to unity at $\eta = -\infty$, the volume fraction of unconverted polymer is severely depleted just to the left of the interface as a result of the chemical reaction. The steep gradients that are produced by even this modest value of k are a good indication of the difficulty of the computational problem.

Of course, the primary item of practical interest is not the form of the concentration profiles but rather the value of the interfacial velocity u, which is obtained as part of the solution. Figure 5 shows the computed variation in $v = -u$ with the rate constant k for fixed values of m and $\mathcal{D}^-$ (the same as in Fig. 4) and three sets of values of χ_{12} and χ_{13}. In each case, the two χ values correspond to limited and complete solubility, respectively. Clearly, there are two distinct regimes with respect to the dependence of v on k. When the latter is large, v varies roughly as $k^{0.5}$ but is nearly independent of the interaction parameters. This is intuitively reasonable: if the reaction does indeed cause a conversion from low solubility to complete solubility, then v should be determined largely by the rate of this conversion, and the precise values of the thermodynamic parameters should be irrelevant. On the other hand, if k is sufficiently small, then v is essentially independent of k but strongly dependent on χ_{12}; there can be no dependence on χ_{13} because the reaction producing species 3 does not occur. In this regime, it is clear that v is determined largely by the solubility of the unconverted polymer, as this provides the driving force for transport through the liquid layer.

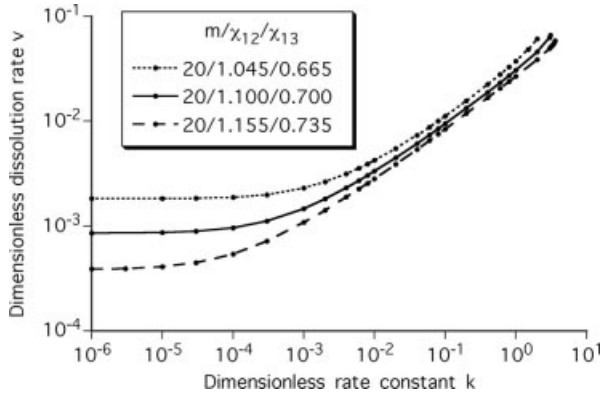

Figure 5 Computed dissolution rate v as a function of reaction rate constant k for $m = 20$, $\mathcal{D}^- = 10^{-4}$, and three sets of interaction parameters.

To complete the analysis, we must know how v varies with m and $\mathcal{D}^-$ in the large-k regime and with χ_{12}, m, and $\mathcal{D}^-$ in the small-k regime. From the aforementioned arguments, we would expect the value of m to be irrelevant when k is large, as long as the diffusivities are held constant. Figure 6 provides some evidence that this is true. On the other hand, because $\mathcal{D}^-$ governs the rate at which the converted polymer can diffuse to the interface, its value should be important. Figure 7 shows that v varies roughly as $(\mathcal{D}^-)^{0.5}$ over a range of conditions; the exponent is actually somewhat smaller than this, but a value of 0.5 might be expected theoretically and will be used for simplicity. Turning to the small-k regime, we first note that v is rigorously independent of $\mathcal{D}^-$ for $k = 0$. This is not obvious but will be proven in the later discussion. Here it suffices to say that the dissolution problem is much simpler when the chemical reaction is absent, and it can be solved for v without a value being specified for $\mathcal{D}^-$. Of course, v does still depend on m and $\chi_{12} \equiv \chi$; in fact, it varies roughly exponentially with each, as shown in Figures 8 and 9. More precisely, $\ln v$ is roughly linear in the quantity $m(\alpha - \beta\chi)$,

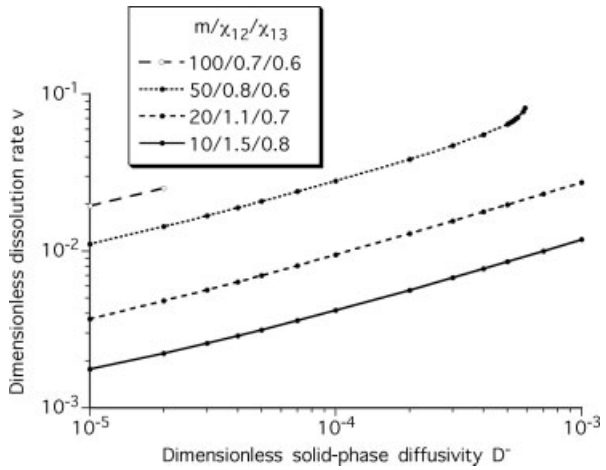

Figure 7 Computed dissolution rate υ as a function of solid-phase diffusivity $\mathscr{D}^-$ for $k = 0.1$ and four sets of Flory–Huggins parameters.

where α and β are constants. This is presumably the way in which the polymer solubility varies with m and χ according to the Flory–Huggins theory.

An overall expression for the dissolution rate υ as a function of the system parameters can now be formulated. We first revert to dimensional quantities by replacing υ, k, and $\mathscr{D}^-$ with $v\delta^+/\mathscr{D}^+$, $k\delta^{+2}/\mathscr{D}^+$, and $\mathscr{D}^-/\mathscr{D}^+$, respectively. The desired expression must then have the form

$$\frac{\upsilon\delta^+}{\mathscr{D}^+} = F\left(\frac{k\delta^{+2}}{\mathscr{D}^+}, \frac{\mathscr{D}^-}{\mathscr{D}^+}, m, \chi\right) \tag{28}$$

where χ again refers to χ_{12}. Recall that χ_{13} has been shown to be irrelevant and F is a function to be determined. Equation (28) is basically a statement of the Buckingham π theorem for this problem. Now, because the expression for υ that describes the large-k regime will be negligible for small k, and vice versa, one can simply add the two formulas to obtain a result that is valid for all k values. According to the previous discussion, this should have the form

$$\frac{\upsilon\delta^+}{\mathscr{D}^+} = A_{(k)}\left(\frac{k\delta^{+2}}{\mathscr{D}^+}\right)^{0.5}\left(\frac{\mathscr{D}^-}{\mathscr{D}^+}\right)^{0.5} + A_{(0)}\exp[m(\alpha - \beta\chi)] \tag{29}$$

or more simply

$$\upsilon = A_{(k)}(k\mathscr{D}^-)^{0.5} + A_{(0)}\frac{\mathscr{D}^+}{\delta^+}\exp[m(\alpha - \beta\chi)] \tag{30}$$

where $A_{(k)}$ and $A_{(0)}$ are constants yet to be determined. Interestingly, the first term in eq. (30) resembles the familiar flame speed formula from combustion theory, whereas the second term describes simple diffusion through a stagnant liquid film. It is rather remarkable that each term involves only one of the two diffusivities.

According to the reptation theory described in references 11 and 12, the diffusivity in a solid polymer network should vary roughly as the inverse square of the chain length, so we take $\mathscr{D}^- \sim m^{-2}$. The situation with respect to the liquid phase is not so simple. According to Flory,[13] the diffusivity in a polymer solution at infinite dilution should vary roughly as $m^{-0.5}$, but it is not clear that this limiting law will apply under realistic conditions. Furthermore, the film thickness δ^+ in eq. (30) will itself depend on $\mathscr{D}^+$, and hence m, in an unknown manner. Therefore, it will be assumed here that the ratio $\mathscr{D}^+/\delta^+$ varies as $m^{-\lambda}$, where the exponent λ is a constant to be determined. With these stipulations, eq. (30) becomes

$$\upsilon = B_{(k)}k^{0.5}m^{-1} + B_{(0)}m^{-\lambda}\exp[m(\alpha - \beta\chi)] \tag{31}$$

where $B_{(k)}$ and $B_{(0)}$ are new constants.

The origins of the temperature dependence of the dissolution rate can be identified from eq. (31). First,

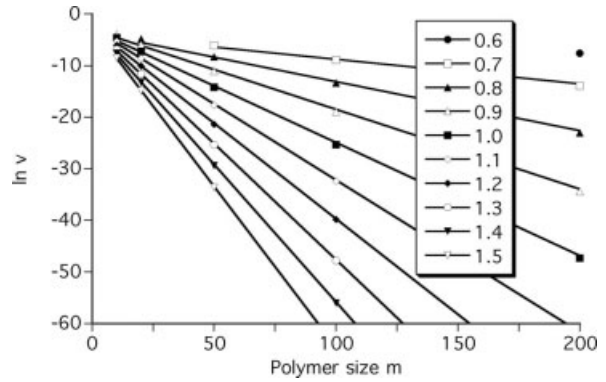

Figure 8 Computed unassisted dissolution rate υ as a function of m for various values of χ.

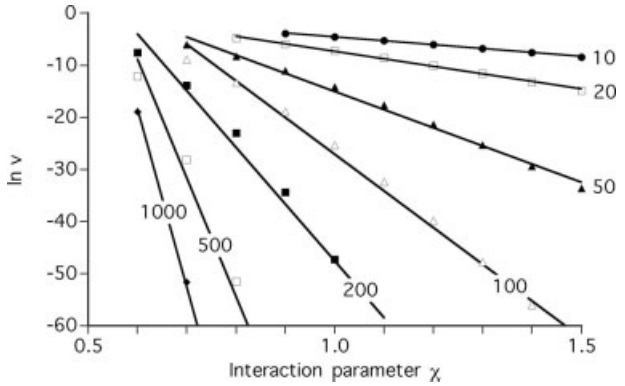

Figure 9 Computed unassisted dissolution rate υ as a function of χ for various values of m.

rate constant k is expected to involve an ordinary Arrhenius factor:

$$k = k_0 \exp\left(-\frac{E_{(k)}}{RT}\right) \tag{32}$$

where $E_{(k)}$ is the activation energy and k_0 is the preexponential factor. It is probable that the reptation-based diffusivity $\mathcal{D}^-$ also has an activation energy. This may or may not be significant with respect to chemically based $E_{(k)}$, but in any case the two activation energies can simply be combined, according to eq. (30). The remaining temperature dependence in υ arises from the fact that the interaction parameter χ is related to the polymer–solvent interchange energy w by[8]

$$\chi = \frac{w}{RT} \tag{33}$$

Making these substitutions in eq. (31) gives

$$\upsilon = B_{(k)} k_0^{0.5} \exp\left(-\frac{E_{(k)}}{2RT}\right) m^{-1} + B_{(0)} m^{-\lambda} \exp\left[m\left(\alpha - \beta\frac{w}{RT}\right)\right] \tag{34}$$

This equation predicts that the overall activation energy for the process will not be a constant, for two distinct reasons. First, there will be a change in value accompanying the transition from the small-k regime to the large-k regime. Second, even when the first term in eq. (34) is negligible, the activation energy will vary as a result of its proportionality to m, which must depend on the absorbed X-ray dose Q. The way in which k_0 and m vary with Q is the last piece of information needed to obtain an expression for υ solely in terms of measurable quantities. This leads us to develop a simple model for the structural changes in PMMA that are produced by exposure to X-ray irradiation.

PHOTOCHEMISTRY MODEL

The effects on PMMA of exposure to X-rays and similar types of radiation have been studied by a number of investigators.[14–21] Although the picture is not entirely clear, there is a reasonable consensus on the principal events that occur.[22] The initial absorption of radiation seems to lead to a scission (or chemical transformation) of the ester side chain of a monomer segment. This results in an excited polymer molecule that can be stabilized either by hydrogen abstraction, which leaves the polymer chain intact, or by a main-chain scission at the β location. Main-chain scissions can also occur by a more direct route, but this is not considered here. Crosslinking reactions, though possible in PMMA,[23,24] are thought not to be important at the doses normally used in LIGA.[25] Thus, we will use the following very simple and schematic mechanism for the radiation-induced changes in PMMA:

A → B: irradiation and ester-group scission.
B → C: stabilization by hydrogen abstraction.
B → C + S: main-chain scission.

The species A, B, and C represent an untouched polymer segment (monomer unit), an excited segment (from which the ester group has been removed), and a stabilized segment (also missing the ester group), respectively. The species S is not a physical entity but merely provides a convenient way of keeping count of the total number of polymer molecules. Denoting the first-order rate constants for the three reactions as k_1, k_2, and k_3, respectively, and using the standard steady-state approximation for species B, one can easily solve the time-dependent kinetic equations for the concentrations of the other species. This gives

$$A = A_0 e^{-k_1 t} \tag{35}$$

$$C = A_0(1 - e^{-k_1 t}) \tag{36}$$

$$S = S_0 + \frac{k_3}{k_2 + k_3} A_0(1 - e^{-k_1 t}) \tag{37}$$

where the subscript 0 denotes the initial value. The quantity $k_3/(k_2 + k_3)$ is the ratio of the main-chain and ester-group scission rates and will henceforth be denoted by r. In addition, S_0 is essentially equal to the initial concentration of polymer molecules and can therefore be written as $A_0 W/M_0$, where W is the molecular weight of the monomer and M_0 is the initial average molecular weight of the polymer. It follows that

$$S = A_0\left[\frac{W}{M_0} + r(1 - e^{-k_1 t})\right] \tag{38}$$

The average chain length of the polymer molecules at any time t is therefore

$$m = \frac{1}{W/M_0 + r(1 - e^{-k_1 t})} \tag{39}$$

Because the rate constant k_1 is proportional to the radiation intensity (dose rate), the quantity $k_1 t$ is proportional to the total dose Q, and we can write

$$\frac{1}{m} = \frac{1}{m_0} + r(1 - e^{-\gamma Q}) \tag{40}$$

where γ is another constant to be determined. In terms of the limiting chain length m_∞ at an infinite dose, eq. (40) becomes

$$\frac{1}{m} = \frac{1}{m_\infty} - \left(\frac{1}{m_\infty} - \frac{1}{m_0}\right)e^{-\gamma Q} \tag{41}$$

where

$$\frac{1}{m_\infty} = \frac{1}{m_0} + r \tag{42}$$

Equation (41) is equivalent to the result proposed by Schmalz et al.,[25] but the derivation here is much simpler. The exponential dependence on Q contrasts with the often-used linear relation that is obtained by the assumption of a fixed scission yield,[26–28] although eqs. (40) and (41) are, of course, linear for small values of Q.

Because m_0 is generally a very large number, eq. (40) shows that the final chain length will be independent of the initial value, except when the dose is very small. Pantenburg et al.[29] showed that this approximation is valid under the conditions normally encountered in LIGA, so it will be adopted here. Therefore, we obtain

$$\frac{1}{m} = r(1 - e^{-\gamma Q}) \equiv rf(Q) \tag{43}$$

From eq. (36), the number of side-chain scissions can be expressed equally simply:

$$C = A_0 f(Q) \tag{44}$$

Equations (43) and (44) are the results needed to complete the development of the preceding section. As already noted, a fundamental assumption of the model is that the removal of side chains during irradiation renders a polymer molecule susceptible to a reaction with the solvent. It follows that pre-exponential factor k_0 in eq. (32) should depend on the number of side chains removed. We would not necessarily expect k_0 to be strictly proportional to C, but a power-law dependence with an unspecified exponent p is a reasonable assumption. Using this along with eqs. (43) and (44) in eq. (34) gives

$$\upsilon = D_{(k)}[f(Q)]^{p/2+1}\exp\left(-\frac{E_{(k)}}{2RT}\right) + D_{(0)} \times [f(Q)]^{\lambda}\exp\left[\frac{1}{rf(Q)}\left(\alpha - \beta\frac{w}{RT}\right)\right] \tag{45}$$

where $D_{(0)}$ and $D_{(k)}$ are still more constants. This cumbersome expression can be simplified by the combination of constants wherever possible:

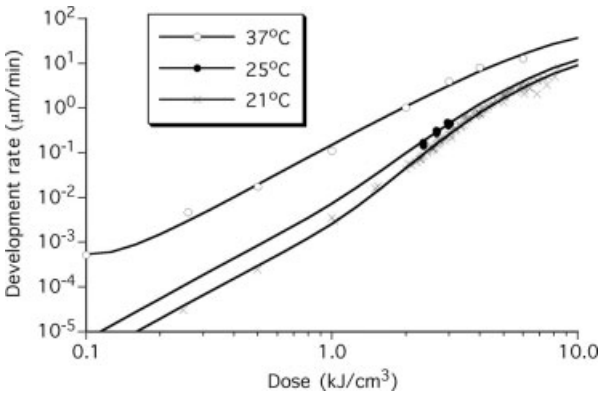

Figure 10 Fit of the reaction-assisted dissolution model to the experimental development rates.

$$\upsilon = C_1[f(Q)]^{C_4}\exp\left(-\frac{C_3}{T}\right) + C_6[f(Q)]^{C_2} \exp\left[\frac{1}{f(Q)}\left(C_7 - \frac{C_8}{T}\right)\right] \tag{46}$$

where

$$f(Q) = 1 - \exp(-C_5 Q) \tag{47}$$

Equation (46) is actually quite similar to the expression proposed by Pantenburg et al.,[29] the main difference here being the presence of $f(Q)$ in the argument of the second exponential. This represents the effect of the polymer molecular weight on the solubility and is a key feature of this model. Unfortunately, most of the constants C_i do not have simple physical meanings, but it should be noted that

$$C_2 = \lambda \tag{48}$$

$$C_3 = \frac{E_{(k)}}{2R} \tag{49}$$

$$C_4 = \frac{p}{2} + 1 \tag{50}$$

These relations provide at least a limited opportunity to check the credibility of inferred values for C_i.

DATA FITTING

We now test the suitability of eq. (46) (and, by inference, the overall model) by fitting it to a set of experimental data. Obviously, because the equation contains a large number of unknown parameters, an extensive database must be employed if the exercise is to have any meaning. The data to be used here are the same as those recently considered by Pantenburg et

TABLE I
Inferred Values of the Constants in Equation (46)

Parameter	Value	Units
C_1	$(3.0 \pm 0.7) \times 10^{25}$	m/s
C_2	4.3 ± 0.1	None
C_3	$(2.3 \pm 0.2) \times 10^{4}$	K
C_4	3.1 ± 0.1	None
C_5	0.183 ± 0.003	cm^3/kJ
C_6	$(6.8 \pm 0.6) \times 10^{-7}$	m/s
C_7	13.68 ± 0.02	None
C_8	$(4.21 \pm 0.09) \times 10^{3}$	K

al.[29] and are shown as the discrete points in Figure 10. As described in more detail in ref. 28, the dissolution rates at 37°C were obtained for thin sheets of commercially available noncrosslinked PMMA that were exposed at the ELSA accelerator in Bonn, Germany. Because the deposited dose was nearly constant across the thickness of each sample, the dissolution rate was independent of time and could be measured simply by the weight difference. On the other hand, most of the data for development temperatures of 21 and 25°C refer to thick sheets of linear cast PMMA that were exposed at the Advanced Light Source at Lawrence Berkeley Laboratory. Dissolution rates were obtained more indirectly by the periodic measurement of the developed depth and the numerical differentiation of the results. The absorbed dose at a given depth was computed via the LEX code written at Sandia National Laboratories (Livermore, CA); this allowed each measured dissolution rate to be associated with a specific value of the dose. Altogether, dissolution rates were measured for doses ranging from approximately 0.1 to 9 kJ/cm^3, and the rates themselves varied over nearly six orders of magnitude, from 3×10^{-5} to 13 $\mu m/min$. They should, therefore, provide a reasonable test of the model.

The data fitting is accomplished via a nonlinear least-squares technique that makes use of the minimization routine in a Microsoft Excel spreadsheet. The logarithms of the dissolution rates are used in the calculations to ensure that the relative errors are small even at low doses. The results of this procedure are shown in Figure 10. The model provides a fairly good qualitative and quantitative fit to the measured rates for all conditions, although the results for 37°C are somewhat inferior. The overall root-mean-square error in $\ln v$ is 0.151, so the average relative error in the predicted rate is approximately 15%. This is almost certainly within the scatter of the data, although some of the individual errors are of course considerably larger.

The optimized values of the constants C_i are given in Table I. The uncertainty stated with each value is the amount by which it can be changed (while the others are held fixed) without the overall root-mean-square error increasing by more than 10% of its optimum value. Of course, this does not account for the possibility that several of the constants could be changed simultaneously by amounts larger than these without the quality of the fit being degraded.

From eq. (49), activation energy $E_{(k)}$ is approximately 380 kJ/mol, which is much too large[30] for the kind of saponification reaction hypothesized by Schmalz et al.[5] (Of course, the apparent activation energy is only half this value.) This suggests that the reptation process does in fact have a very significant activation energy of its own. The exponent p in eq. (45) has a value of 4.2, according to eq. (50). This seems rather large for a reaction order and suggests that an exponential dependence of the rate constant k on the number of side-chain scissions might be more appropriate than a power law. In fact, it could be argued that the removal of the side chains reduces the steric hindrance to attack by the solvent molecules and is thus an energetic effect that should be reflected in the activation energy rather than the pre-exponential factor. However, making this assumption actually leads to a substantial degradation in the fit to the data; in particular, the observed behavior for low doses at 21°C cannot be reproduced.

DISCUSSION

It is clear from Figure 10 that the model is least successful in fitting the data at the highest temperature, especially at low doses. The unwanted curvature in this region, which is absent at the low temperature, is responsible for much of the overall error if the obvious outliers at 21°C are disregarded. To gain some insight into this problem, it is useful to examine the relative contributions made to the dissolution rate by the two terms in eq. (46). A plot of this nature is shown in Figure 11. Clearly, at both 21 and 25°C, the reaction-assisted process is the dominant contributor at low

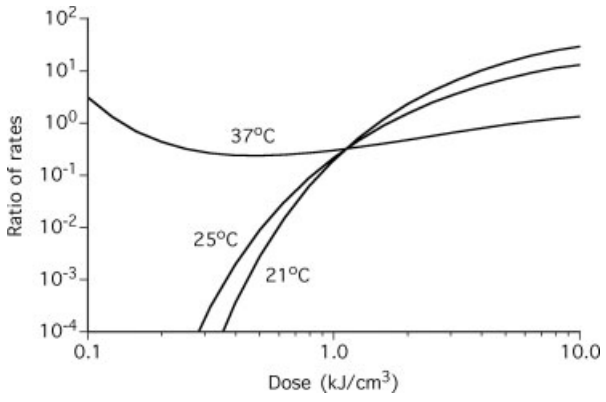

Figure 11 Inferred ratio of the conventional dissolution rate to the reaction-assisted dissolution rate as a function of the dose and temperature.

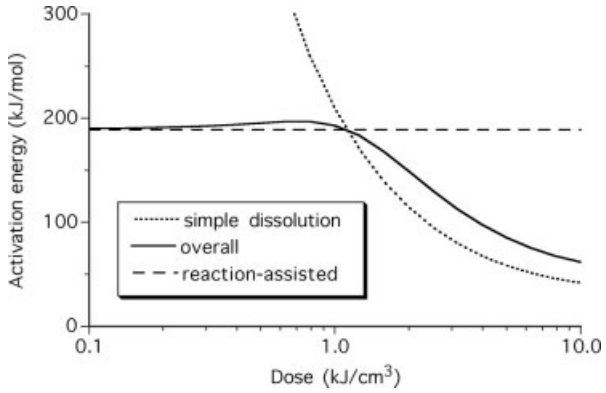

Figure 12 Activation energies inferred from the fit to the development rate data.

doses, whereas dissolution of the unreacted (but still irradiated) polymer is the preferred route at high doses. This appears to reflect the extreme sensitivity of the polymer solubility to the molecular weight: when the dose is low, the molecular weight is so large that dissolution cannot occur until the reaction takes place and converts the polymer into a highly soluble form. On the other hand, at high doses, the molecular weight is low enough to provide good solubility, and dissolution occurs so quickly that the reaction has little opportunity to contribute. The situation is very different at 37°C, however; in this case, the two contributions are roughly comparable at all doses, so the preceding arguments must no longer apply. This can be explained by the fact that the argument of the second exponential in eq. (46) changes sign at a temperature of approximately 35°C if the inferred values of C_7 and C_8 are used. Therefore, above this temperature, the severe decrease in solubility with increasing polymer size no longer occurs, and the chemical reaction is no longer necessary to dissolve large molecules. The existence of such a critical temperature is perfectly consistent with Figure 2 if one recalls that the interaction parameter χ is inversely proportional to T [cf. eq. (33)]. However, because eq. (46) actually describes increasing solubility with the polymer size at temperatures above the critical value, the model is not expected to be valid at very low doses. This probably explains the nonmonotonic behavior at 37°C in Figure 11 as well as the unwanted curvature in Figure 10.

Referring again to Figure 11, we find that the reaction-assisted process influences the high-dose dissolution rate more strongly at 37°C than it does at the lower temperatures, undoubtedly because of a difference in activation energies. Figure 12 shows the overall apparent activation energy for dissolution as well as the values for the two contributing processes. The overall values were obtained from Arrhenius plots generated from eq. (46) for fixed values of the dose; the upper limit of the temperature range was set at 35°C to avoid including the anomalous behavior noted previously. Obviously, the plot mirrors the experimental fact that the overall activation energy varies strongly with the dose, but only in the upper part of the range. According to the model, this behavior arises from both the transition in the dominant process and the effect of m on the solubility, as noted in the discussion following eq. (34). Because the activation energy for unassisted dissolution is relatively small at high doses, the reaction-assisted process becomes a more important contributor as the temperature increases.

Despite the complexity of the model presented here, there are several areas in which it could in principle be improved. One potential flaw arises from the fact that the solvent is treated as a single species. By assumption, this species is consumed by its chemical reaction with the polymer, whereas in reality some components of the developer solution would likely remain intact. It could, therefore, be argued that the model underestimates the extent of penetration of the solvent into the solid phase. However, it appears that solvent penetration plays only a minor role in determining the rate of dissolution, contrary to intuition. In fact, it can be proven that the dissolution rate is completely independent of any solid-phase dynamics if the postulated chemical reaction does not occur. To see this, note that the system involves only two species if there is no reaction to produce species 3. According to the phase rule, the equilibrium interfacial concentrations are then fixed for a given temperature and pressure; they can be computed before the differential equations governing the process are solved. There are now only two such independent equations, so only two boundary conditions are needed for each phase. For the liquid phase, we have the pure-solvent condition at the right-hand boundary in addition to the known composition at the interface, so the problem is self-contained and can be solved by itself for the desired flux, that is, the dissolution rate. This obviously implies that the rate is independent of the solid-phase diffusivity, and this observation is consistent with the second term of eq. (30). In the gel layer, the composition profile simply adjusts itself to be consistent with the flux determined by the liquid-phase problem, although it should be noted that this adjustment is possible only because the solid-phase outer boundary condition is applied at $\eta = -\infty$. In any case, it appears that the key effect of the chemical reaction is to alter the interfacial composition in a way that favors dissolution. This probably explains why increases in the rate constant always lead to increases in the dissolution rate, even as they simultaneously reduce the extent of solvent penetration into the polymer.

Just as the developer should in theory be treated as a multicomponent liquid, the polymer should be treated as a mixture of molecules of different sizes.

Because the solubility, in particular, is such a strong function of the chain length, the polydispersity of the polymer could in general have a significant effect on the dissolution behavior. However, if the range of initial molecular weights and the range of doses are such that eq. (43) is an acceptable approximation, then the polydispersity of the original polymer is no longer an issue. To take it into account would require a vast increase in the complexity of the model, and there seems to be no compelling reason to do so. Essentially, all existing work in this area does, in fact, assume a unimodal polymer.

Finally, it could be argued that the use of the Flory–Huggins theory in modeling LIGA is questionable because it was originally intended to describe nonpolar systems, and the chemicals composing the GG developer do not belong to this category. However, because the simulations of dissolution dynamics have been used simply to suggest a suitable form for the rate expression, the details of the thermodynamics are probably not critical. The gross features of the Flory–Huggins theory can be assumed to apply well enough that the general conclusions are still valid.

CONCLUSIONS

The X-ray exposure and development steps of the LIGA process are quite complex, and the model presented here is without question a simplification. Unlike most previous descriptions of polymer dissolution, however, it is physically based rather than largely empirical, and it accounts for chemical effects that appear to be unique to LIGA. The fact that the model fits the experimental database so well is encouraging, although it certainly does not prove that all details of the model are correct. Perhaps the main contribution of the model is giving a plausible explanation for the change in the behavior of the dissolution rate with increasing dose; the data strongly suggest that there is a transition from one governing process to another, and the model reproduces this quite well. It is somewhat unfortunate that the number of adjustable parameters is so large, but the opportunities to measure these quantities independently appear to be very limited. The value inferred for C_5 agrees reasonably well with that quoted by Pantenburg et al.,[29] but little can be said beyond this. In any case, it is unlikely that the data could be fit successfully with less than the eight parameters used here. On the other hand, it is also unlikely that using additional parameters would result in much improvement, so there is little to be gained by an attempt to account for other experimental variables such as the dose rate. At this point, it would be most helpful to have additional evidence supporting the existence of the chemical effects proposed by Schmalz et al.,[5] and an experimental program to accomplish this is currently underway at Sandia.

References

1. Papanu, J. S.; Soane, D. S.; Bell, A. T.; Hess, D. W. J Appl Polym Sci 1989, 38, 859.
2. Papanu, J. S.; Hess, D. W.; Soane, D. S.; Bell, A. T. J Appl Polym Sci 1990, 39, 803.
3. Herman, M. F.; Edwards, S. F. Macromolecules 1990, 23, 3662.
4. Hasko, D. G.; Yasin, S.; Mumtaz, A. J Vac Sci Technol B 2000, 18, 3441.
5. Schmalz, O.; Hess, M.; Kosfeld, R. Angew Makromol Chem 1996, 239, 93.
6. Newman, J. S. Electrochemical Systems, 2nd ed.; Prentice Hall: Englewood Cliffs, NJ, 1991; p 265.
7. Flory, P. J. Principles of Polymer Chemistry; Cornell University Press: Ithaca, NY, 1953; p 549.
8. Prausnitz, J. M. Molecular Thermodynamics of Fluid-Phase Equilibria; Prentice Hall: Englewood Cliffs, NJ, 1969; p 292.
9. Petzold, L. R. Sandia National Laboratories Report SAND82–8637; Sandia National Laboratories: Livermore, CA, 1982.
10. Hildebrand, J. H.; Scott, R. L. The Solubility of Nonelectrolytes, 3rd ed.; Dover: New York, 1964.
11. de Gennes, P. G. Scaling Concepts in Polymer Physics; Cornell University Press: Ithaca, NY, 1979; p 227.
12. de Gennes, P. G.; Léger, L. Annu Rev Phys Chem 1982, 33, 49.
13. Flory, P. J. Principles of Polymer Chemistry; Cornell University Press: Ithaca, NY, 1953; p 629.
14. Choi, J. O.; Moore, J. A.; Corelli, J. C.; Silverman, J. P.; Bakhru, H. J Vac Sci Technol B 1988, 6, 2286.
15. Ichikawa, T.; Yoshida, H. J Polym Sci Part A: Polym Chem 1990, 28, 1185.
16. Moore, J. A.; Choi, J. O. Radiation Effects on Polymers; ACS Symposium Series 475; American Chemical Society: Washington, DC, 1991; p 156.
17. Zhang, X.; Jacobsen, C.; Lindaas, S.; Williams, S. J Vac Sci Technol B 1995, 13, 1477.
18. Wollersheim, O.; Zumaqué, H.; Hormes, J.; Kadereit, D.; Langen, J.; Häussling, L.; Hoessel, P.; Hoffmann, G. Nucl Instrum Methods Phys Res Sect B 1995, 97, 273.
19. Ichikawa, T. Nucl Instrum Methods Phys Res Sect B 1995, 105, 150.
20. Wollersheim, O.; Hormes, J. Chem Phys 1996, 204, 129.
21. Henry, A. C.; McCarley, R. L.; Das, S.; Khan Malek, C.; Poche, D. S. Microsyst Technol 1998, 4, 104.
22. Schmalz, O.; Hess, M.; Kosfeld, R. Angew Makromol Chem 1996, 239, 79.
23. Lehockey, E. M.; Wice, J. D.; Reid, I. Can J Phys 1987, 65, 975.
24. Lehockey, E. M.; Reid, I.; Hill, I. J Vac Sci Technol A 1988, 6, 2221.
25. Schmalz, O.; Hess, M.; Kosfeld, R. Angew Makromol Chem 1996, 239, 63.
26. Greeneich, J. S. J Electrochem Soc 1974, 121, 1669.
27. Greeneich, J. S. J Electrochem Soc 1975, 122, 970.
28. Pantenburg, F. J.; Achenbach, S.; Mohr, J. J Vac Sci Technol B 1998, 16, 3547.
29. Pantenburg, F. J.; Bankert, M. A.; Domeier, L. A.; Griffiths, S. K.; Wepfer, K. C. Presented at the 5th Biennial Workshop on High Aspect Ratio Micro-Structure Technology, Monterey, CA, 2003.
30. Daly, J.; Lenz, R. W. J Appl Polym Sci 1992, 46, 847.